Spread and Rebound of Liquid Droplets upon Impact on Flat Surfaces

Ted Mao, David C. S. Kuhn, and Honghi Tran
Pulp & Paper Centre, Dept. of Chemical Engineering and Applied Chemistry, University of Toronto, 200 College St., Toronto, M5S 1A4, Canada

The spread and rebound of droplets upon impact on flat surfaces at room temperature were studied over a wide range of impact velocities (0.5–6 m/s), viscosities (1–100 mPa·s), static contact angles (30–120°), droplet sizes (1.5–3.5 mm), and surface roughnesses using a fast-shutter-speed CCD camera. The maximum spread of a droplet upon impact depended strongly on the liquid viscosity and the impact velocity. The tendency of a droplet to deposit or to rebound is determined primarily by the liquid viscosity and the liquid/substrate static contact angle. A model more broadly applicable than existing models was developed to predict maximum spread as a function of the Reynolds number, the Weber number, and the static contact angle. Based on the conservation of energy, a rebound model is proposed that predicts the tendency to rebound as a function of maximum spread and static contact angle.

The maximum-spread model prediction agrees to within 10% with more than 90% of the experimental data from different sources. In the current study, the rebound model successfully predicts the tendency of a droplet to rebound.

Introduction

The spread of liquid droplets upon impact on a rigid surface has been studied by many researchers. The spread area covered by a droplet is an important process parameter in ink-jet printing, spray coating, precision solder dispensing, and spray cooling.

When a droplet is not captured by the impact surface, droplet rebound occurs. In other applications the prevention of rebound is important, such as in pesticide spraying on foliar surfaces, whereas rebound is advantageous when rain falls on a nonwetting fabric, and for the avoidance of ash-deposit buildup on heat-exchanger tubes in recovery boilers in the pulp and paper industry. Understanding the criteria that control droplet rebound is of great importance in avoiding heat-exchanger fouling.

The maximum extent to which a droplet spreads is a crucial parameter in predicting rebound. There are two approaches to modeling the maximum spread. The numerical approach simulates the transient flow field during droplet spread using computational fluid dynamics codes. Examples are the work of Harlow and Shannon (1967), Trapaga and Szekely (1991), Fukai et al. (1993, 1995), and Pasandideh-Fard et al. (1996). The theoretical approach assumes velocity profiles in a droplet upon impact, and applies mass and energy conservation between the point of impact and the maximum spread to solve for the maximum spread diameter. Examples are the work of Jones (1971), Madejski (1976), Chandra and Avedisian (1991), Asai et al. (1993), Pasandideh-Fard et al. (1996). Bennett and Poulikakos (1993) reviewed some of the theoretical models in detail. Recently, Scheller and Bousfield (1995) proposed a squeeze-flow model using a force balance to estimate the maximum spread.

Although the rebound phenomenon has been reported in many experiments, few theoretical analyses of rebound have been conducted. Worthington (1876) observed rebound when a milk droplet fell onto a smoked glass plate. Wachters and Westerling (1966), Chandra and Avedisian (1991), Qiao and Chandra (1996) reported significant rebound when a droplet impacted on a heated substrate surface whose temperature was above the Leidenfrost temperature, that is, the temperature at which a vapor film is formed between the liquid and the substrate. Fukai et al. (1995) demonstrated both numerically and experimentally the occurrence of droplet rebound. Ford and Furmidge (1967) studied the recoil of spray droplets on foliar surfaces experimentally and theoretically.

To date, theoretical models have not addressed the effect of substrate surface properties adequately. The viscous dissi-

pation energy, a critical value in the calculation of spread and rebound, has been estimated empirically from limited experimental data, and few systematic experimental studies of rebound have been made.

The present work examines experimentally the effects of impact parameters on maximum spread and rebound, and previous maximum-spread models are refined, and a rebound model is presented that predicts the tendency of a liquid droplet to rebound upon impact. Sequences of calibrated images are shown of the impact process as liquid droplets strike flat surfaces and rebound. The effects of velocity (0.5–6 m/s), viscosity (1–100 mPa · s), static contact angle (30–120°), droplet size (1.5–3.5 mm), and surface roughness were studied. Since maximum spread is a crucial intermediate step in the quantification of rebound, a detailed theoretical analysis of the maximum spread is given. The theoretical estimation of viscous dissipation energy is presented along with an empirical correlation used to define it. In contrast to previous models, the proposed maximum spread model accounts for the wettability of the substrate surface using the static contact angle. The model predictions agree with more than 90% of the experimental data to within 10% for a wide range of applications. A rebound model based on the energy conservation is also presented that predicts the tendency of rebound as a function of the maximum spread and the static contact angle.

Due to the applicability of the maximum-spread model over a wide parametric range, the results of this study are relevant to a broad range of processes, including ink-jet printing, spray coating, precision solder dispensing, and spray cooling. In particular, it is hoped that the results of this study will be applicable to the fouling of heat-exchanger tubes by molten-ash droplets in kraft recovery boilers in the pulp and paper industry. In the superheater region of such boilers, the flue gas is laden with 0.1- and 3-mm-diameter molten alkali salt particles, called carryover, which are carried by the flue gas at velocities up to 7 m/s. Some of these particles deposit on tube surfaces upon impact, while others bounce off. By incorporating the effects of heat transfer and the strike angle, the present rebound model can be used to predict the tendency of molten droplets to stick to tube surfaces.

Experimental Setup and Procedure

The experimental setup for the droplet impact study is shown in Figure 1. A droplet was generated by forcing the test fluid through a flat-tipped stainless-steel needle (25G5/8) using a syringe pump (Model 100, KD Scientific Corp.). The liquid flow rate was adjusted so that individual droplets first formed at the tip of the needle, then detached and fell due to the force of gravity. The droplet was enclosed in a vertical, 2-in.-o.d. Plexiglass tube to protect it from air currents. Before a droplet struck a substrate surface, it moved through an infrared beam between the emitter and the detector of an optical trigger (MAZOF VIS II Trigger System). The 5-V pulse generated by the trigger went to a time/counter board (CIO-CTR05, ComputerBoards, Inc.) in an IBM-compatible personal computer, which sent a 5-V pulse to activate the shutter of a charge coupled device (CCD) camera after a preset time delay. The time delay varied so that images were taken at different times after the initial droplet impact. The images were stored in a digital format and downloaded to the

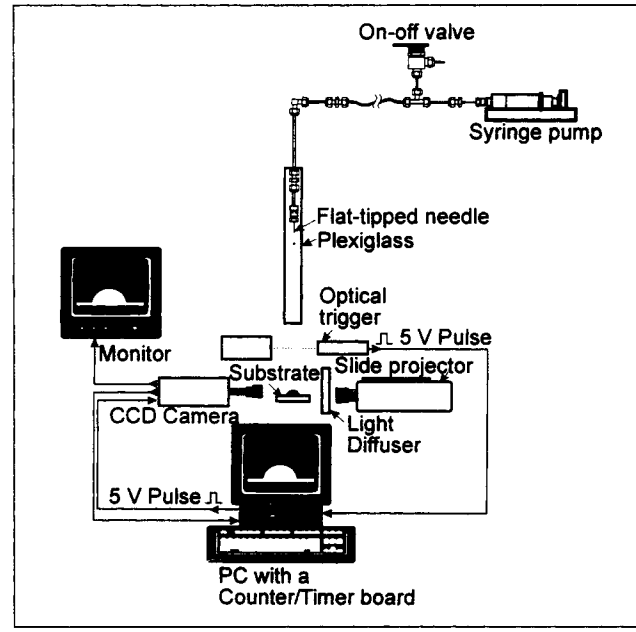

Figure 1. Experimental apparatus of droplet impact.

computer for analysis. A sequence of pictures describing the impact process was created from individual images of many droplets taken at different time delays.

The fast-shutter CCD camera (FlashCam, Optikon Corp.) has a multiple-exposure feature and is capable of taking pictures at shutter speeds as fast as 1 μs. Up to 10 images can be superimposed on a single frame with a time delay of 1 μs to 1 ms between individual exposures. The shutter speed was set between 10 μs and 20 μs so as to take sharp pictures without a sophisticated illumination system. Using the multiple exposure feature, droplet impact velocity and the rate of deformation upon impact were precisely determined.

The camera was positioned on a one-dimensional translation stage (Newport Corp.) and a rotatable platform (Newport Corp.). The focus of the camera was adjusted using the one-dimensional stage, while the rotatable platform allowed the camera to be aligned at an angle of 0° to 90° to the horizontal. A reversed 50-mm C-Mount lens was used together with extension tubes to improve image sharpness at a magnification greater than one. The magnification was manipulated so that the image could accommodate the maximum spread of the droplet.

A backlighting technique was employed using a Kodak Carousel projector (Model 4200) that has an opal glass diffuser in order to produce a uniform, bright, diffused light source. No noticeable temperature rise in test substrates was detected when they were exposed to this light source during the testing period.

Mixtures of water and sucrose were used as test fluids; viscosity was measured using a HAAKE Rotovisco RV12 viscometer. Fluid density was determined from the mass of fluid contained in a volumetric flash. The measurements agreed with data in the literature (Weast, 1981) to within 2%. Since the droplet diameter is a function of needle outside diameter, liquid density, and surface tension, the surface tension was back-calculated from the droplet diameter, needle outside diameter, and the liquid density (Adamson, 1976).

Three smooth substrates were used: a smooth glass slide, a polished stainless-steel plate, and a paraffin wax block. The stainless-steel plate was polished using 600-grit emery cloth and mirror finished using 6 μm Leco premium diamond suspension (Leco Corp.). The paraffin wax block was polished using 600-grit emery cloth. In contrast, rough substrates were polished using low-grit emery cloth and without polishing. Long rectangular pieces of substrate were used so that they could be easily advanced to expose a fresh surface for the next droplet impact. A substrate surface could accommodate at least five droplets before being washed with double-distilled water and being dried with KimWipes EX-L tissue paper prior to reuse.

The droplet velocity just before impact was calculated from a series of superimposed images having a preset time delay between exposures. The velocity was also calculated based on the free-fall distance from the tip of the needle to the substrate surface. The discrepancy between the two methods varied with free-fall distance, but was generally less than 3%.

The diameter of a droplet was measured from the droplet image just before impact, using image-analysis software. The droplet was not perfectly spherical, although the difference between the horizontal and vertical dimensions was less than 4%. The equivalent droplet diameter $D = \sqrt[3]{D_x^2 D_y}$, where D_x is the diameter of the horizontal dimension and D_y is the diameter of the vertical dimension, was calculated based on mass conservation, assuming that the droplet is axisymmetrically elliptical with respect to the vertical y axis. The spherical droplet diameter was also calculated from the mass of 10 droplets of known density. The results obtained from the two methods were in agreement to within 2%.

Because the experiment is highly reproducible, it is valid to use the videography technique to describe the sequence of events in droplet impact. Since the droplet impact is a rapid deformation process, the precision of timing and spatial measurement of deformation determines the experimental reproducibility. Systematic timing errors have three major sources. First, a free-fall droplet is subject to periodic oscillation (Clift et al., 1978), and is affected by air currents and vibrations. The resulting margin of error is 40 μs. Second, errors can result if the optical trigger beam and the droplet trajectory are not well aligned. Third, because the trigger does not produce a sharp 5-V pulse to the CIO-CTR05 timer/counter board controlled by a 7-MHz crystal clock, a maximum error of 2 μs may result. Thus, the overall timing error is about 50 μs. However, since the camera is capable of taking 10 exposures per frame, the current system can resolve the impact process to within 5 μs. This is equivalent to recording a single droplet impact at 200,000 images per second. Spatial error is mainly caused by optical distortion. The optical components were calibrated using a calibration graticule (E-10, Leica Canada) and a spherical stainless ball of known diameter. The measured maximum spread diameter upon impact was found to be precise to within 2% from ten replications of one experiment.

Results and Discussion

Impact process

Figure 2 shows the impact sequence of a 2.7-mm water droplet on a paraffin wax surface at room temperature. The

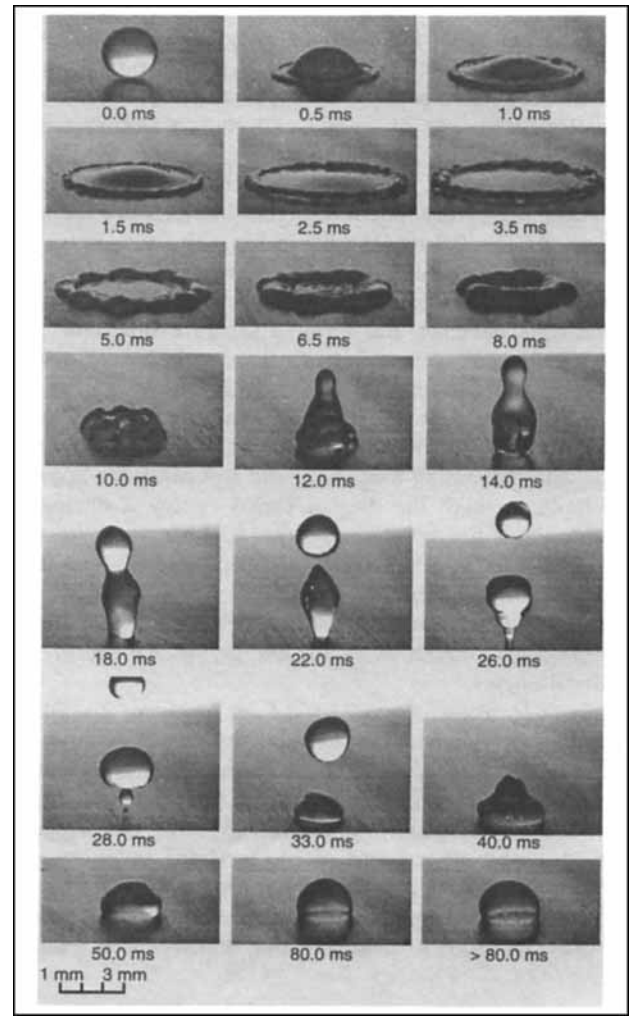

Figure 2. Impact sequence of a 2.7-mm water droplet on a paraffin wax surface at a velocity of 1.58 m/s.

camera is aimed 15° below the horizontal in order to obtain clear images of the droplet spread upon impact. The impact velocity was 1.58 m/s with an associated droplet Reynolds number, $Re = \rho u D/\mu$, of 4257, and Weber number, $We = \rho u^2 D/\gamma_{LV}$, of 92. The static contact angle was 96°.

At $t = 0.0$ ms, just before impact, the droplet is clearly spherical in shape. It deforms and spreads rapidly upon impact in the radial direction, out from the point of impact beneath the droplet, due to the rapid pressure increase at the point of impact (Huang et al., 1973). A raised rim is formed at the periphery at $t = 0.5$ ms due to surface-tension forces that limit the spread and decelerate the radial flow close to the periphery. After $t = 2.5$ ms, the rate of spread slows down, and the central liquid pool thins out and continues to feed liquid into the rim, which forms a series of liquid lobes. At $t = 3.5$ ms, the droplet reaches its maximum spread and is momentarily at rest because of the depletion of kinetic energy. The initial impact energy of the droplet is dissipated in overcoming viscous flow and in producing new surface area.

After the droplet reaches maximum spread, pairs of liquid lobes at the periphery join, and a 10-lobed annulus is formed.

This moves back toward the center, that is, recoils ($t = 5.0$ ms), as a result of the large surface energy of the droplet–solid system. At the same time, concentric ripples propagate inward on the surface of the central lake of liquid. From $t = 5.0$ to 10.0 ms, the area of liquid–solid contact shrinks rapidly causing the lobes in the rim to fuse and the rim to swell, and to move inward until the rim reaches the center. This marks the beginning of the rebound of the droplet from the solid surface. At $t = 12.0$ ms, the liquid rises up from the center and assumes a roughly conical shape as the area of liquid–solid contact further decreases. At $t = 22.0$ ms, the tip of the cone detaches and forms a separate subdroplet. Finally, the contact area shrinks to zero as the whole droplet rebounds from the wax surface ($t = 28.0$ ms).

Under the influence of gravity, the droplet fall back to the wax surface, and further droplet spread and recoil sequences occur with decreasing amplitude and frequency for approximately 40 ms until the droplet excess energy is dissipated. Equilibrium is finally achieved at $t \approx 80.0$ ms.

Four distinct stages involved in the impact–rebound process are shown in Figure 3:

Stage a Before Impact: t = 0.0 ms in Figure 2. The droplet impact energy consists of kinetic energy, surface energy, and potential energy;

Stage b Maximum Spread: t = 3.5 ms in Figure 2. This is the point at which the liquid flow changes direction from spreading outwards to recoiling inwards. The surface energy of the droplet is at a maximum, while the kinetic energy is zero. The potential energy in both stages a and b is negligible compared with other forms of energy (Ford and Furmidge, 1967). A characteristic length that is proportional to the surface energy is the liquid–solid contact diameter d_m, that is, the maximum-spread diameter, and is normalized with respect to the original droplet diameter D to give a maximum spreading factor d_m/D;

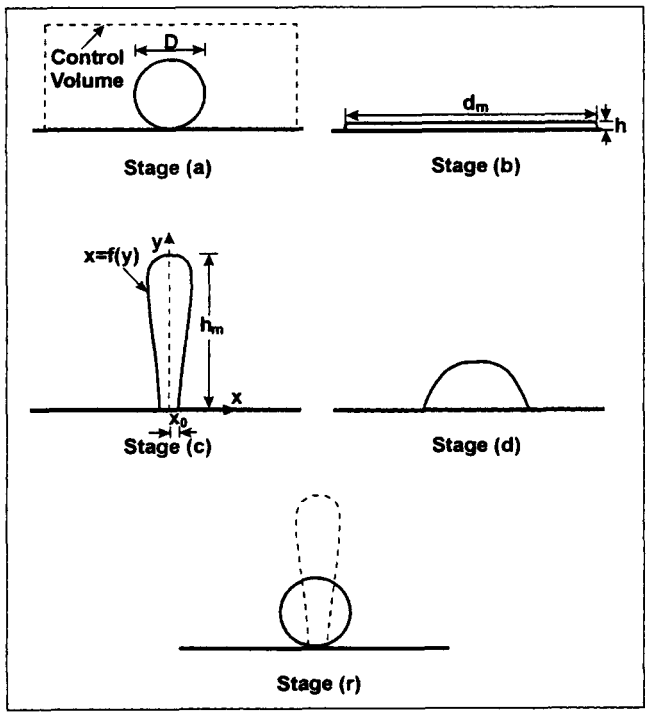

Figure 3. Four stages of the impact process and one criterion.

Stage c Maximum Recoil/Rebound: t = 28.0 ms in Figure 2. At this moment, the droplet changes its direction of motion from up to down under the influence of gravity. This stage signifies the maximum extent to which a droplet recoils upwards, and the droplet possesses potential and surface energy but no kinetic energy;

Stage d Equilibrium: t > 80.0 ms in Figure 2. The droplet possesses a minimum energy that is equal to the static surface energy.

A fictitious stage c configuration is introduced as stage r, *rebound criterion*, where the droplet, with its original spherical shape, is in a position just above the substrate and momentarily at rest. In this case the droplet upward acceleration is counterbalanced by gravity. However, if the energy possessed by a droplet in stage c is greater than in stage r, the droplet will further pop up and be swept away by the strong shear force of the flue gas in the context of fouling on heat exchanger tubes by molten droplet impact. Therefore, a rebound criterion is formulated: a droplet bounces off the surface if the energy possessed in stage c is greater than that in stage r. Conversely, the droplet remains on the surface if the energy is lower in stage c than in stage r.

Effect of substrate surface

Figure 4 shows the effect of the substrate surface on the impact process. Separate 2.7-mm water droplets impact on a paraffin wax block, a stainless-steel plate, and a glass slide at a velocity of 0.85 m/s. The camera is aligned to the horizontal, and is set to take three exposures of a droplet upon impact, with a time delay of 180 μs between each of the 20 μs exposures.

From 0.0 ms to 6.0 ms, the droplet deformation is similar in these three cases. Each reaches the maximum spread at $t = 6.0$ ms, the each attains almost the same radius. Therefore, the deformation and spreading of the droplet from the point of impact, that is, stage a, to the maximum spread, that is, stage b, is dominated by the inertial and viscous forces, and the effect of the substrate is minor. This is in agreement with the observation of Scheller and Bousfield (1995).

Table 1 compares the maximum spread on the three substrates, which shows that although the substrate does not significantly affect the maximum spread, its effect does exist. Under the same impact conditions, the maximum spread of a water droplet on the glass slide is consistently larger than that on the stainless-steel substrate, and both are larger than that on the paraffin wax block. Ford and Furmidge (1967) also found that the maximum spread increased with decreasing contact angle.

In Figure 4, after $t = 6.0$ ms, the flattened droplets start to recoil. The droplet on the wax surface recoils much faster than droplets on the other two surfaces. At $t = 12.0$ ms, a large value of the dynamic contact angle is observed at the wax–water–air interface on the wax surface; the peripheral surface tension forces squeeze the droplet upward. In contrast, the area of liquid–solid contact decreases slowly on the stainless-steel plate and even more slowly on the glass slide. In the latter two cases, as the central portion of the fluids moves upward, some liquid remains at the periphery; only

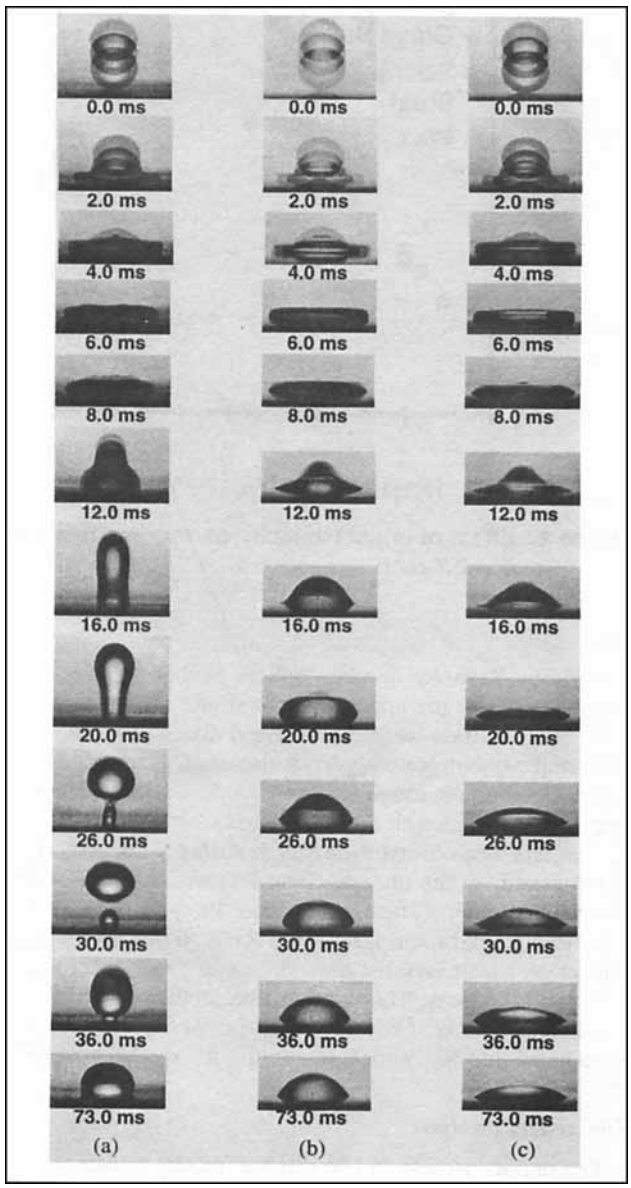

Figure 4. Impact of a 2.7 water droplet on (a) the paraffin wax block; (b) the stainless-steel plate; (c) the glass slide.

small values of the dynamic contact angle are observed at the solid–water–air interfaces.

After $t = 12.0$ ms, the water droplet bounces off the wax surface in a similar way to that shown at $t = 12.0$ to 28.0 ms in Figure 2. In the case of the stainless-steel substrate, only spread–recoil oscillations are observed, and in the case of the glass substrate, there are smaller and less frequent spread–recoil oscillations. In all three cases, the droplet reaches equilibrium after its excess energy is completely dissipated; however, it takes much longer to reach equilibrium on the wax surface than on the other two surfaces. This indicates that energy is dissipated more slowly in the water droplet–wax substrate system than in the other two systems.

In the equilibrium state, the shape of the liquid meniscus is different for different substrates: the static contact angles θ of the water droplet on the wax, stainless-steel, and glass surfaces are 97°, 67°, and 37°. For a given liquid, the contact angle characterizes the energy level of the solid surface. In general, the contact angle indicates the surface energetics of the solid–liquid–vapor system or wettability (Neumann, 1974).

Table 1. Data of the Maximum Spread on Three Substrate Surfaces

Case	Impact Vel. (m/s)	d_m/D (a) Paraffin Wax Static Contact Angle $\theta = 97°$	(b) Stainless Steel $\theta = 67°$	(c) Glass Slide $\theta = 37°$
1	0.55	1.65	1.67	1.77
2	0.82	2.10	2.16	2.20
3	1.00	2.26	2.34	2.53
4	1.58	3.01	3.09	3.11
5	1.86	3.60	3.67	3.70
6	2.77	4.32	4.42	4.50
7	3.72	4.78	4.88	4.94

Effect of viscosity

Droplet viscosity is an important variable affecting the impact process. In Figure 5, droplets with viscosities of 1.0 mPa·s, 2.0 mPa·s, and 16.4 mPa·s impact on the paraffin wax surface at a velocity of 2.0 m/s. No significant difference is seen during the initial rapid deformation stage ($t < 0.6$ ms) because the inertial force of impact is much larger than the viscous force. However, as the droplets approach their maximum spread and the rate of spread decreases, the viscous effect begins to play a dominant role. The energy dissipated during droplet spread increases with increasing viscosity, thus the maximum spread for a given impact energy decreases inversely with increased viscosity, as shown in Figure 5 at $t = 2.4$ ms.

A droplet with higher viscosity produces smaller maximum spread; it thus has less energy available for recoil and/or rebound. Moreover, its excess surface energy must overcome higher viscous dissipation during recoil and/or rebound. Therefore, the tendency of droplets to recoil and rebound is less for higher viscosity liquids than for lower viscosity liquids. Figure 5 shows that there is significant rebound in the case where the droplet viscosity is 1.0 mPa·s, whereas the droplet with a viscosity of 2.0 mPa·s only just bounces off the surface. In contrast, the droplet with a viscosity of 16.4 mPa·s undergoes limited recoil and no rebound. At the end of the impact process, the droplets in all three cases have approximately the same contact angle on the paraffin wax surface.

Effect of impact velocity

Figure 6 plots the data in Table 1 and shows that the maximum spread increases with increasing impact velocity, which leads to an increase in the maximum energy available for recoil and/or rebound. However, there is a corresponding increase in viscous dissipation attributed to wall shear stress on the extended area of liquid–solid contact. The balance of these two factors determines the overall effect of impact velocity on recoil and/or rebound.

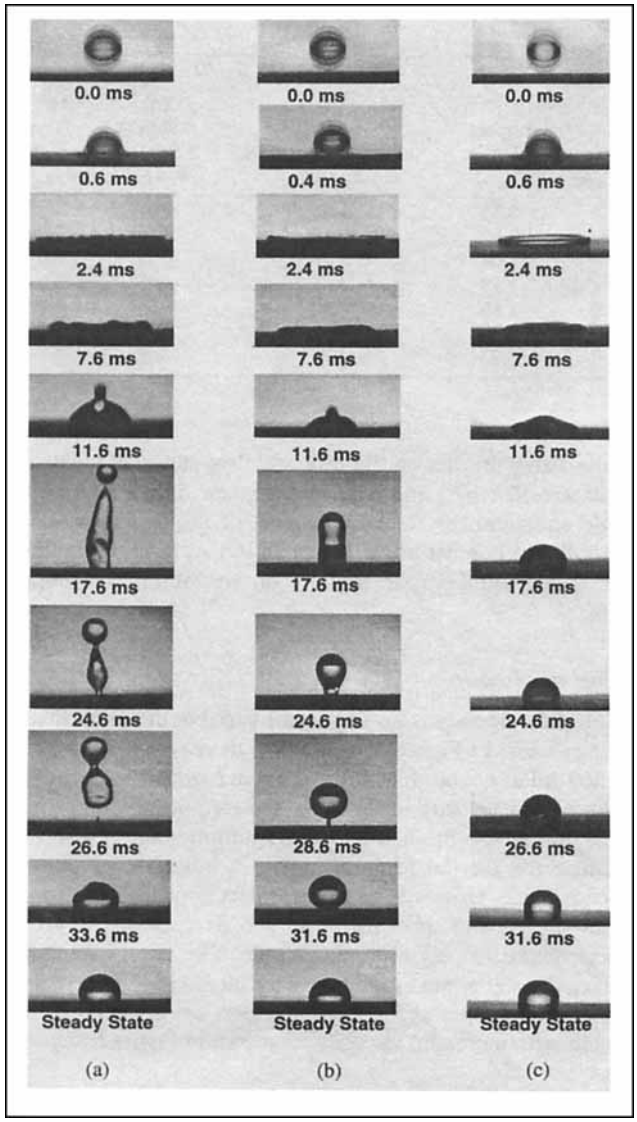

Figure 5. Impact of (a) a water droplet (1.0 mPa·s), D = 2.7 mm, u_{Imp} = 2.0 m/s; (b) a 20% sucrose solution droplet (2.0 mPa·s), D = 2.6 mm, u_{Imp} = 2.0 m/s; (c) a 50% sucrose solution droplet (16.4 mPa·s), D = 2.5 mm, u_{Imp} = 2.0 m/s on the paraffin wax surface.

The effect of impact velocity on rebound is illustrated in Figure 7, which shows a 2.7-mm water droplet impacting on the paraffin wax surface at velocities of 0.55 m/s, 1.86 m/s, 2.77 m/s, and 4.53 m/s. In the first case, the droplet does not rebound from the surface, whereas in the second and third cases, the droplet rebounds higher as the impact velocity is increased. However, the droplet shatters or splashes in the fourth case (at $t = 0.7$ ms) even before it reaches maximum spread.

Effect of droplet size and surface roughness

Several experiments were conducted to investigate the effect of droplet size on the impact process. Although the droplet diameter is an important parameter, it is embedded

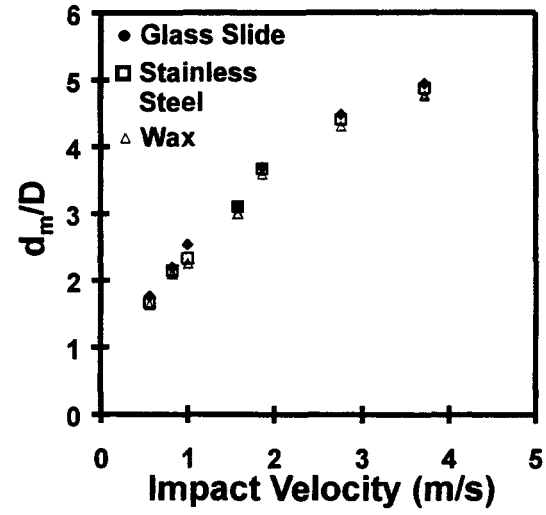

Figure 6. Effect of impact velocity on maximum spread, D = 2.7 mm.

in both the Reynolds number and the Weber number, which directly relate to the maximum spread and rebound.

Rough substrate surfaces polished using low-grit emery cloth and without polishing were also used. It was found that liquid droplets on rough surfaces produced smaller contact angles than on smooth surfaces. Nonaxisymmetric spreading of droplets was observed on rough surfaces because of the heterogeneity of the surfaces. Fine droplets also remained on the wetted rough surface after recoil. In spite of these complexities, the maximum spread and rebound of a droplet upon impact on rough surfaces have the same general features as on smooth surfaces. They can also be predicted by the models described later. Only the rough-surface contact angle is introduced into the models to account for surface roughness.

Theoretical analysis

The impact process can be divided into four distinct stages (Figure 3, discussed previously). Based on the conservation of energy between stages a and b, and stages b and c, models of maximum spread and rebound were developed.

Stage a, Before Impact. Energy is conserved in the system defined by a control volume (Figure 3) that contains a liquid droplet, a solid surface, and the surrounding atmosphere. The energy level of the solid surface is defined as zero as a reference for the system. Kinetic energy, surface energy, and potential energy in the control volume are considered in the following analysis.

Just before impact, the droplet possesses both kinetic energy (K_a) and total surface energy (S_a), but negligible potential energy (Ford and Furmidge, 1967). Because the solid surface energy is the reference and is set to zero, the total surface energy consists of only the liquid–vapor surface energy ($S_{a,LV}$), that is, the product of the droplet surface area (A) and the liquid–vapor surface tension (γ_{LV}). The total impact energy E_{Impact} is the sum of the kinetic energy and the surface energy:

$$E_{\text{Impact}} = K_a + S_a; \tag{1}$$

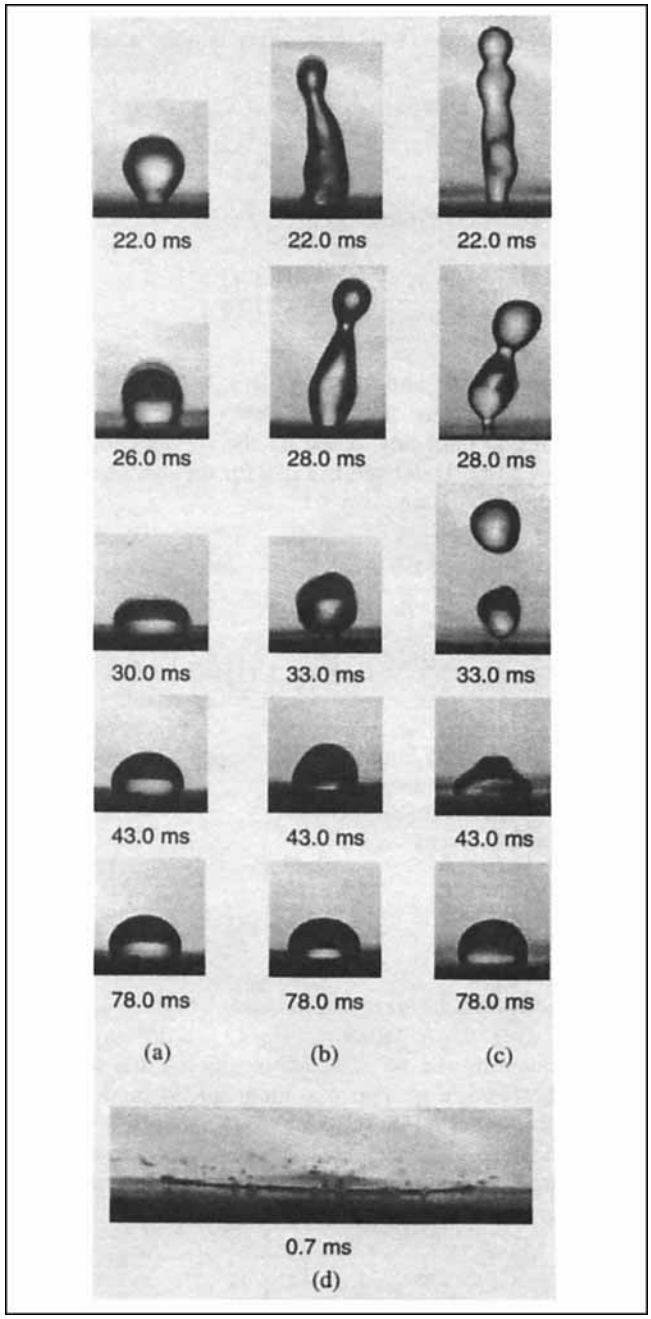

Figure 7. Impact of a 2.7-mm water droplet on the paraffin wax surface at (a) u_{Imp} = 0.55 m/s; (b) u_{Imp} = 1.86 m/s; (c) u_{Imp} = 2.77 m/s; (d) u_{Imp} = 4.53 m/s.

$$K_a = \left(\frac{1}{2}\rho u^2\right)\left(\frac{1}{6}\pi D^3\right); \tag{2}$$

$$S_a = S_{a,LV} = A\gamma_{LV} = \pi D^2 \gamma_{LV}, \tag{3}$$

where ρ is the liquid density, u is the impact velocity, and D is the droplet diameter.

Stage b, Maximum Spread. After impact, the kinetic energy is consumed in increasing the area of the liquid–vapor and solid–liquid interfaces, and in overcoming viscous forces as the droplet distorts and flattens. At the moment of maximum spread (d_m), the kinetic energy (K_b) of the flattened droplet is assumed to be zero, since it is negligible compared with the surface energy:

$$K_b = 0. \tag{4}$$

The flattened droplet is assumed to be a thin circular disk with a top surface area of $(\pi/4)d_m^2$, a height (h) of $^2/_3(D^3/d_m^2)$, and a circumferential edge area of $^2/_3\,\pi(D^3/d_m)$. The surface energy, S_b, is the sum of the liquid–vapor surface energy, $S_{b,LV}$, and the energy of the new solid–liquid surface, $S_{b,SL}$, minus the solid–vapor surface energy, $S_{b,SV}$, which has been lost in the process:

$$S_b = S_{b,LV} + S_{b,SL} - S_{b,SV}$$
$$= \left(\frac{\pi}{4}d_m^2 + \frac{2}{3}\pi\frac{D^3}{d_m}\right)\gamma_{LV} + \frac{\pi}{4}d_m^2(\gamma_{SL} - \gamma_{SV}), \tag{5}$$

where γ_{SL} is the solid–liquid surface tension and γ_{SV} is the solid–vapor surface tension.

Because the values of γ_{SL} and γ_{SV} are not readily available, Young's equation (Young, 1855) was used to relate their difference, $\gamma_{SL} - \gamma_{SV}$, to γ_{LV} and the static contact angle θ:

$$\gamma_{LV}\cos\theta = \gamma_{SL} - \gamma_{SV}. \tag{6}$$

Here, the static contact angle should be used, since it is uniquely related to the surface tensions, which are thermodynamic properties. A dynamic contact angle such as the advancing contact angle used by Ford and Furmidge (1967) and Pasandideh-Fard et al. (1996) is not applicable in this type of analysis.

Substituting Eq. 6 into Eq. 5 gives

$$S_b = \left[\frac{\pi}{4}d_m^2(1-\cos\theta) + \frac{2}{3}\pi\frac{D^3}{d_m}\right]\gamma_{LV}. \tag{7}$$

Since the kinetic energy in stage b is zero, the total energy is equal to the surface energy:

$$E_b = S_b. \tag{8}$$

The energy conservation between stage a and stage b can now be established as:

$$K_a + S_a = S_b + \mathrm{Diss}_{a\text{-}b}, \tag{9}$$

where $\mathrm{Diss}_{a\text{-}b}$ is the energy consumed by viscous dissipation of the droplet in going from stage a to stage b.

As shown earlier, K_a, S_a, and S_b have been defined with an unknown, d_m. Thus, Eq. 9 can be used to solve for d_m if $\mathrm{Diss}_{a\text{-}b}$ is quantified. However, no complete model exists to describe $\mathrm{Diss}_{a\text{-}b}$, although many researchers have attempted to approximate it, for example, Madejski (1976), Asai et al. (1993), and Karl et al. (1993). The following is the develop-

ment of a theoretical estimation and an empirical correlation of the dissipation energy.

The present model is based on the work of Chandra and Avedisian (1991):

$$\text{Diss}_{a\text{-}b} = \int_0^{t_c}\int_V \phi\, dV dt \approx \phi V t_c, \tag{10}$$

where the dissipation function is given by

$$\phi = \mu\left(\frac{\partial v_i}{\partial x_j} + \frac{\partial v_j}{\partial x_i}\right)\frac{\partial v_i}{\partial x_j} \approx \mu\left(\frac{du}{dy}\right)^2, \tag{11}$$

where du/dy is the normal velocity gradient in the boundary layer. The volume of the viscous layer is $V = (1/4\,\pi d_m^2)\delta$, where δ is the boundary-layer thickness. The time, t_c, taken for a droplet to spread from stage a to stage b is estimated by $t_c = {}^8/_3(D/u_{Imp})$, where u_{Imp} is the impact velocity (Pasandideh-Fard et al., 1996). The time from initial impact to maximum spread was derived by Pasandideh-Fard et al. following a conservation of mass approach assuming the droplet spreads into a cylindrical disk.

The flow field of a droplet impinging on a solid surface is approximated by a stagnation-point flow in the present study, shown in Figure 8. A stagnation-point flow considers the momentum change from the normal direction to the tangential direction and boundary layer development in the tangential direction. The boundary-layer thickness is calculated using the analytical solution to the stagnation-point flow. However, calculations show that for highly viscous liquids, the boundary-layer thickness, δ, is larger than the flattened droplet height, h. Consequently, the volume of the viscous layer is modified to $V = {}^1/_4(\pi d_m^2)h$. Thus boundary-layer thicknesses of $\delta < h$ and $\delta > h$ need to be considered separately, and are defined for simplicity as low- and high-viscosity regimes, respectively. These regimes cannot be simply characterized by the Reynolds number, since the boundary-layer thickness is not only affected by viscosity and impact velocity but also the maximum spread. The velocity profile throughout the viscous layer is assumed to be linear in both regimes, leading to a constant normal velocity gradient, but also a nonzero tangential stress at the liquid–gas interface. It will be shown that this simplification does not seriously affect the quality of the resulting semiempirical equation used to calculate d_m/D.

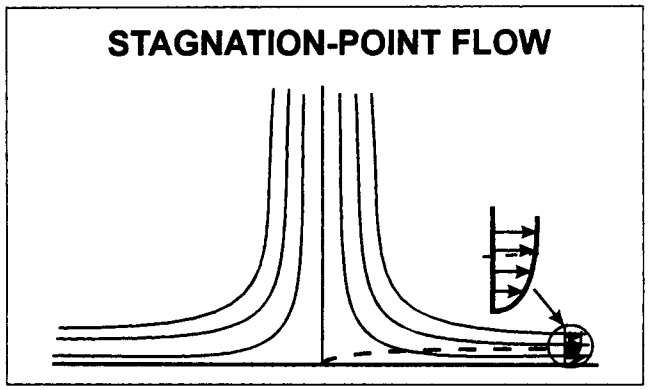

Figure 8. Boundary layer of a stagnation-point flow.

Therefore, a theoretical viscous dissipation model is developed for two regimes: for low-viscosity liquids, where $\delta < h$:

$$\frac{\text{Diss}_{a\text{-}b}}{\pi D^2 \gamma_{LV}} = 0.35\frac{We}{\sqrt{Re}}\left(\frac{d_m}{D}\right)^2; \tag{12}$$

and for high-viscosity liquids, where $\delta > h$:

$$\frac{\text{Diss}_{a\text{-}b}}{\pi D^2 \gamma_{LV}} = 0.53\frac{We}{Re}\left(\frac{d_m}{D}\right)^4; \tag{13}$$

where $Re = \rho u D/\mu$ and $We = \rho u^2 D/\gamma_{LV}$. The quantitative description of viscous dissipation now makes it possible to calculate d_m/D implicitly, based on the energy conservation from stages a to b as defined in Eq. 9 for the two regimes: for low viscosity liquids, where $\delta \leq h$:

$$\left[\frac{1}{4}(1-\cos\theta) + 0.35\frac{We}{\sqrt{Re}}\right]\left(\frac{d_m}{D}\right)^3 - \left(\frac{We}{12}+1\right)\left(\frac{d_m}{D}\right) + \frac{2}{3} = 0; \tag{14}$$

and for high-viscosity liquids, where $\delta > h$:

$$0.53\frac{We}{Re}\left(\frac{d_m}{D}\right)^5 + \frac{1}{4}(1-\cos\theta)\left(\frac{d_m}{D}\right)^3 - \left(\frac{We}{12}+1\right)\left(\frac{d_m}{D}\right) + \frac{2}{3} = 0. \tag{15}$$

Apparently, two different results can be obtained using Eqs. 14 and 15 when $\delta = h$. Moreover, Eq. 15 is a fifth-order polynomial equation, and no analytical solution exists to obtain d_m/D. Therefore, a general maximum-spread model that is easy to solve is desirable. In order to obtain such a model, a general dissipation model is developed by correlating the present experimental data of both low- and high-viscosity liquids using the model structure of Eq. 12, that is,

$$\frac{\text{Diss}_{a\text{-}b}}{\pi D^2 \gamma_{LV}} = x\frac{We^y}{Re^z}\left(\frac{d_m}{D}\right)^2$$

where x, y, and z are constants to be determined empirically. It is obtained using least square data regression that

$$\frac{\text{Diss}_{a\text{-}b}}{\pi D^2 \gamma_{LV}} = 0.2\frac{We^{0.83}}{Re^{0.33}}\left(\frac{d_m}{D}\right)^2. \tag{16}$$

The resulting equation used to calculate d_m/D is

$$\left[\frac{1}{4}(1-\cos\theta) + 0.2\frac{We^{0.83}}{Re^{0.33}}\right]\left(\frac{d_m}{D}\right)^3 - \left(\frac{We}{12}+1\right)\left(\frac{d_m}{D}\right) + \frac{2}{3} = 0, \tag{17}$$

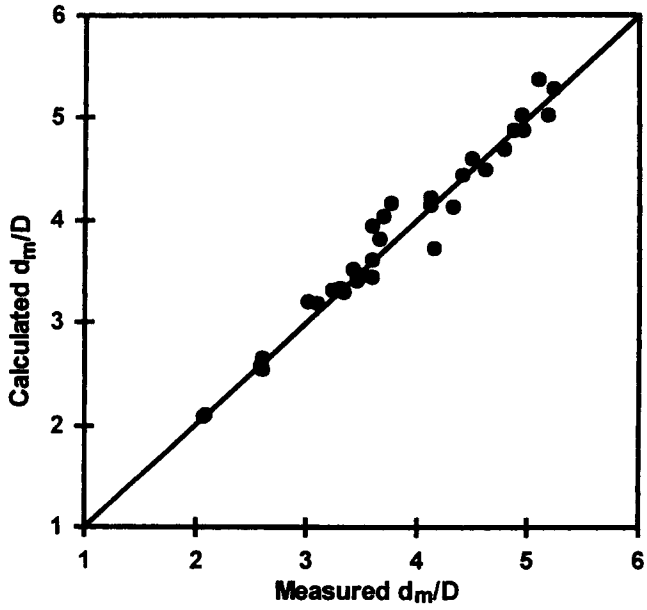

Figure 9. Comparison of the calculated maximum spread using this model (Eq. 17) with the experimental data in this study.

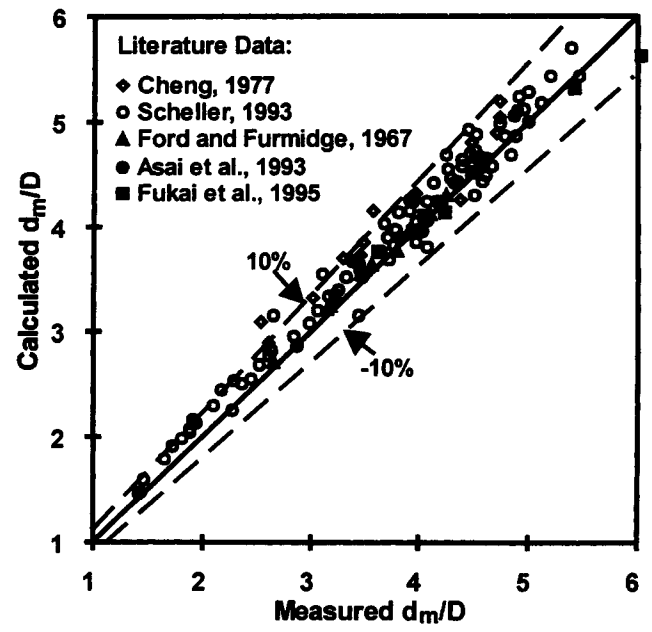

Figure 10. Comparison of the calculated maximum spread using this model (Eq. 17) with the experimental data in the literature.

where d_m/D has an exact solution, since for an equation of $x^3 + px + q = 0$, the real root is given by

$$x = \sqrt[3]{-\frac{q}{2} + \sqrt{\left(\frac{q}{2}\right)^2 + \left(\frac{p}{3}\right)^3}} + \sqrt[3]{-\frac{q}{2} - \sqrt{\left(\frac{q}{2}\right)^2 + \left(\frac{p}{3}\right)^3}}.$$

Figure 9 compares the model predictions (Eq. 17) with the present experimental measurements, and the agreement is to within 10% over a range of impact velocities (1–6 m/s), viscosities (1–100 mPa·s), static contact angles (30–120°), and droplet sizes (1.5–3.5 mm). The limit of this model is that its precision decreases significantly when the impact velocity is less than 1 m/s since the surface tension effect plays an important role in spreading, and the flat disk assumption in stage b and the stagnation-point flow analogy may not be appropriate at low impact velocities. Figure 10 compares the calculated maximum spread using the present model with the data of Cheng (1977), Scheller (1993), Ford and Furmidge (1967), Asai et al. (1993) and Fukai et al. (1995) over a wide range of impact velocities (1.4–28 m/s), viscosities (1–296 mPa·s), surface tensions (25–73 mJ/m^2), static contact angles (34–100°), and droplet sizes (0.04–3.7 mm). The predictions agree with more than 90% of the literature data to within 10%. Figure 11 compares the present model with the literature models for prediction of maximum spread. The measurements are the same literature data as those used in Figure 10. Scheller and Bousfield's model overpredicts maximum spread at small values. The model of Pasandideh-Fard et al. underpredicts maximum spread of high-viscosity liquids because of its improper estimation of the boundary-layer thickness. An advancing contact angle of 90° is assumed in this model when it is not available in the literature. Asai et al.'s model significantly overpredicts maximum spread at large values. It is shown that the present semiempirical model provides better predictions in general, although it overpredicts maximum spread, particularly at small values of maximum spread. This is because the flat disk assumption at stage b does not consider the rim at the periphery and the ripples in the flattened-droplet surface. However, introducing them leads to a much more complicated expression for the maximum spread that is difficult to solve. Based on the predicted maximum-spread value, the energy in stage b, that is, the maximum energy available for recoil and/or rebound, can be

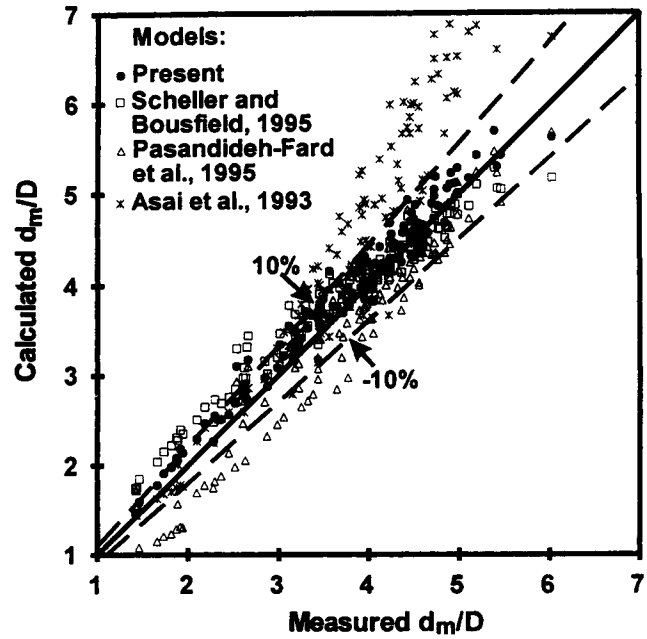

Figure 11. Comparison of maximum-spread predictions using different models with the experimental data in the literature.

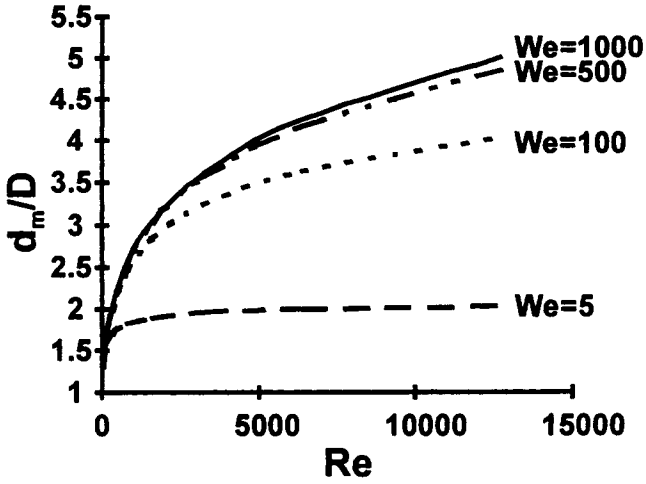

Figure 12. Variation of maximum spread with *Re* and *We*.

calculated using Eq. 7. This is the basis for the development of a rebound model.

Equations 14, 15 and 17 show that the maximum spread is a function of the Reynolds number, the Weber number, and the contact angle. The predicted effects of the Reynolds number and the Weber number using Eq. 17 are illustrated in Figure 12 for the contact angle of 90°. As the Reynolds number and the Weber number increase, the maximum spread increases. Since impact energy increases with increasing the Reynolds number and the Weber number, a higher impact energy must lead to a greater maximum spread.

Stage c, Maximum Recoil/Rebound. Stage c defines the maximum extent to which a droplet recoils or bounces. At this moment, since the droplet is assumed to be at rest and the kinetic energy (K_c) is zero, only the potential energy (P_c) and the surface energy (S_c) are considered.

It is assumed that the droplet in this stage is a body of revolution about the y axis. Thus, the potential energy (P_c) and the surface energy (S_c) are

$$P_c = \pi\rho g\int_0^{h_m} y\cdot x^2\,dy, \tag{18}$$

$$S_c = 2\pi\gamma_{LV}\int_0^{h_m} x\cdot\sqrt{1+[f'(y)]^2}\,dy - \gamma_{LV}\pi x_0^2\cos\theta, \tag{19}$$

where $x = f(y)$, and $f'(y)$ is the first-order derivative with respect to y (see Figure 3). However, the geometric configuration of the liquid body in stage c is not well defined, and thus there is no analytical expression for $x = f(y)$. In this study, P_c and S_c are obtained by numerical integration of the digital profile of a droplet image.

Stage d, Equilibrium. This is the stage where excess energy is completely dissipated through spread–recoil oscillations, and the droplet reaches an equilibrium dictated by minimum surface-energy considerations.

Stage r, Rebound Criterion. This is a fictitious configuration of stage (c) that is used as a measure of rebound. After the deformation and flattening of a droplet upon impact, the excess surface energy enables the droplet to recover its spherical shape and its original diameter. The droplet is just above the solid surface and is considered to be momentarily at rest. Therefore, an energy balance involves the potential energy P_r and the surface energy S_r as follows:

$$P_r = \frac{\pi}{12}\rho g D^4, \tag{20}$$

$$S_r = S_{r,LV} = \pi D^2\gamma_{LV}. \tag{21}$$

Since the potential energy as defined by Eq. 20 never exceeds 2% of the total energy within the broad parametric bounds of the experiments, it is neglecting in the development of the rebound model. Therefore, the total energy in this stage reduces to

$$E_r = S_r = \pi D^2\gamma_{LV}. \tag{22}$$

Rebound occurs when $E_c > E_r$. However, since the geometry of a droplet in stage c is complex, it is difficult to obtain E_c directly. But the energy in stage b E_b can be calculated using Eq. 7 with the maximum spread prediction. Therefore, E_c can be related to E_b and $\text{Diss}_{b\text{-}c}$ from energy conservation considerations between stages b and c:

$$E_c = E_b - \text{Diss}_{b\text{-}c}, \tag{23}$$

where $\text{Diss}_{b\text{-}c}$ is the energy dissipated between stages b and c as the droplet undergoes recoil and/or rebound. Consequently, a rebound criterion can be expressed as

$$E^*_{ERE} \equiv \frac{E_c - E_r}{E_r} = \frac{E_b - \text{Diss}_{b\text{-}c} - E_r}{E_r} > 0, \tag{24}$$

where E^*_{ERE} is defined as the excess rebound energy normalized with respect to the energy possessed in stage (r); and E^*_{ERE} describes the tendency of a droplet to rebound upon impact. A droplet remains on the surface when $E^*_{ERE} \le 0$.

The following empirical correlation of $\text{Diss}_{b\text{-}c}$ as a function of the maximum spread d_m/D and the static contact angle was developed based on the experimental impact data using least-square data regression:

$$\frac{\text{Diss}_{b\text{-}c}}{E_r} = 0.12\left(\frac{d_m}{D}\right)^{2.3}(1-\cos\theta)^{0.63}. \tag{25}$$

Substituting Eqs. 8, 22, and 25 into Eq. 24 results in the proposed rebound model:

$$E^*_{ERE} = \frac{1}{4}\left(\frac{d_m}{D}\right)^2(1-\cos\theta) - 0.12\left(\frac{d_m}{D}\right)^{2.3}(1-\cos\theta)^{0.63} + \frac{2}{3}\left(\frac{D}{d_m}\right) - 1. \tag{26}$$

Figure 13 shows the functionality of the excess rebound energy with maximum spread, d_m/D, and contact angle, θ. When θ is less than 90°, that is, the substrate is wetted by the liquid, E^*_{ERE} decreases with increasing d_m/D. Upon impact on a wettable surface, the more a droplet spreads, the less is

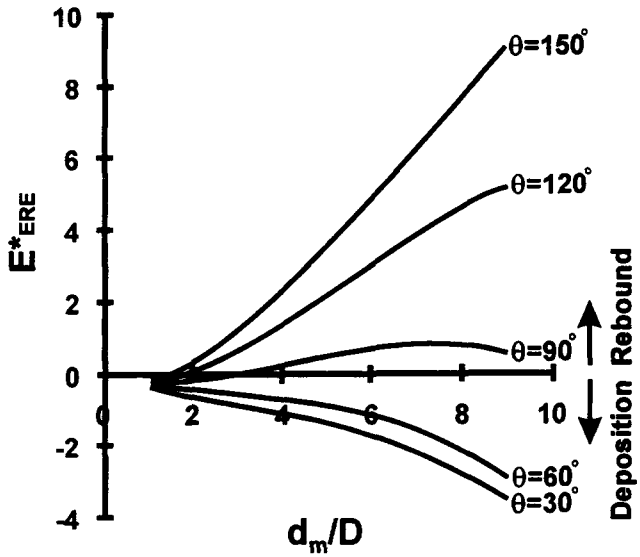

Figure 13. Excess rebound energy as a function of the maximum spread and the static contact angle, using Eq. 26.

the tendency for it to rebound, because more energy is dissipated by viscous flow than is generated by excess surface as a result of droplet deformation. However, when θ is greater than 90°, that is, impact on a nonwetted surface, the tendency of droplet rebound increases as the maximum spread increases and the contact angle increases. This is confirmed by the current experimental observations.

Conclusions

From extensive investigations into the maximum spread and recoil/rebound of liquid droplets upon impact on flat surfaces at room temperature, liquid viscosity and impact velocity were found to be the most important parameters affecting the maximum extent to which a droplet spreads upon impact. Viscosity and static contact angle play a dominant role in determining the tendency of a droplet to rebound after impact.

A semiempirical model was developed to predict the maximum spread as a function of the Reynolds number, the Weber number, and the static contact angle. The maximum spread increases with an increase in the Reynolds number and the Weber number; however, the effect of the contact angle is less important. Predicted results agree with more than 90% of the experimental data from different sources to within 10%. The precise calculation of the maximum droplet spread makes it possible to develop a rebound model, since a droplet possesses the maximum surface energy for recoil and rebound as its maximum spread.

The rebound model so produced predicts that the tendency of the droplet to rebound upon impact is a strong function of the maximum spread and the static contact angle.

Acknowledgments

This work is a part of a research program on "Control of Recovery Boiler Fireside Deposits and Corrosion," jointly sponsored by ABB Power Generation Segment, Ahlstrom Corporation, Babcock & Wilcox Company, Bergemann USA, Champion International Corporation, Diamond Power Specialty Company, E. B. Eddy Forest Products Ltd., Georgia Pacific Corporation, International Paper Company, Irving Pulp & Paper Limited, James River Corporation, Kvaerner Pulping Technologies, Tampella Power Corporation, Union Camp Corporation, Westvaco Corporation, Weyerhaeuser Company, and Willamette Industries, Inc., and the National Sciences and Engineering Research Council of Canada.

Literature Cited

Adamson, A. W., *Physical Chemistry of Surfaces*, Wiley, New York (1976).

Asai, A., M. Shioya, S. Hirasawa, and T. Okazaki, "Impact of an Ink Drop on Paper," *J. Imag. Sci. Tech.*, **37**, 205 (1993).

Bennett, T., and D. Poulikakos, "Splat-quench Solidification: Estimating the Maximum Spreading of a Droplet Impacting a Solid Surface," *J. Mat. Sci.*, **28**, 963 (1993).

Chandra, S., and C. T. Avedisian, "On the Collision of a Droplet with a Solid Surface," *Proc. Roy. Soc. (London)*, A, **432**, 13 (1991).

Cheng, L., "Dynamic Spreading of Drops Impacting onto a Solid Surface," *Ind. Eng. Chem. Process Des. Dev.*, **16**(2), 192 (1997).

Clift, R., J. R. Grace, and M. E. Weber, *Bubbles, Drops, and Particles*, Academic Press, New York (1978).

Ford, R. E., and C. G. L. Furmidge, "Impact and Spreading of Spray Drops on Foliar Surfaces," *Wetting, Soc. Chem. Industry Monograph*, **25**, 417 (1967).

Fukai, J., Z. Zhao, D. Poulikakos, C. M. Megaridis, and O. Miyatake, "Modeling of the Deformation of a Liquid Droplet Impinging Upon a Flat Surface," *Phys. Fluids*, **5**(11), 2588 (1993).

Fukai, J., Y. Shiiba, T. Yamamoto, O. Miyatake, D. Poulikakos, C. M. Megaridis, and Z. Zhao, "Wetting Effects on the Spreading of a Liquid Droplet Colliding with a Flat Surface: Experiment and Modeling," *Phys. Fluids*, **7**(2), 236 (1995).

Harlow, F. H., and J. P. Shannon, "The Splash of a Liquid Droplet," *J. Appl. Phys.*, **38**, 3855 (1967).

Huang, Y. C., F. G. Hammitt, and W. J. Yang, "Hydrodynamic Phenomena during High-speed Collision between Liquid Droplet and Rigid Plane," *J. Fluids Eng.*, **95**, 276 (1973).

Jones, H., "Cooling, Freezing and Substrate Impact of Droplets Formed by Rotary Atomization," *J. Phys. D: Appl. Phys.*, **4**, 1657 (1971).

Karl, A., K. Anders, and A. Frohn, "Experimental Investigation of Droplet Deformation during Wall Collisions by Image Analysis, Experimental and Numerical Flow Visualization," *ASME, FED.*, **172**, 135 (1993).

Madejski, J., "Solidification of Droplets on a Cold Surface," *Int. J. Heat Mass Transfer*, **19**, 1009 (1976).

Neumann, A. W., "Contact Angles and Their Temperature Dependence: Thermodynamic Status, Measurement, Interpretation and Application," *Adv. Coll. Inter. Sci.*, **4**, 105 (1974).

Pasandideh-Fard, M., Y. M. Qiao, S. Chandra, and J. Mostaghimi, "Capillary Effects during Droplet Impact on a Solid Surface," *Phys. Fluids*, **8**(3), 650 (1996).

Qiao, Y. M., and S. Chandra, "Boiling of Droplets on a Hot Surface in Low Gravity," *Int. J. Heat Mass Trans.*, **39**(7), 1379 (1996).

Scheller, B. L., "Drop Formation and the Spreading Behavior of Newtonian and Shear-Thinning Liquid Drops Impacting a Solid Surface," PhD Thesis, Univ. of Maine, Orono (1993).

Scheller, B. L., and D. W. Bousfield, "Newtonian Drop Impact with a Solid Surface," *AIChE J.*, **41**(6), 1357 (1995).

Trapaga, G., and J. Szekely, "Mathematical Modeling of the Isothermal Impingement of Liquid Droplets in Spraying Processes," *Met. Trans. B.*, **22B**, 901 (1991).

Wachters, L. H. J., and N. A. J. Westerling, "The Heat Transfer from a Hot Wall to Impinging Water Drops in the Spheroidal State," *Chem. Eng. Sci.*, **21**, 1047 (1966).

Weast, R. C., M. J. Astle, eds., *CRC Handbook of Chemistry and Physics*, 60th ed., CRC Press, Boca Raton, FL (1981).

Worthington, A. M., "On the Forms Assumed by Drops of Liquids Falling Vertically on a Horizontal Plate," *Proc. Roy. Soc. (London)*, **25**, 261 (1876).

Young, T., *Miscellaneous Works*, I. G. Peacock, ed., Vol. I, Murray, London, p. 418 (1855).

Manuscript received June 4, 1996, and revision received Feb. 6, 1997.